

See discussions, stats, and author profiles for this publication at: <https://www.researchgate.net/publication/24406482>

Nanosized zinc oxide particles induce neural stem apoptosis

Article in *Nanotechnology* · April 2009

DOI: 10.1088/0957-4484/20/11/115101 · Source: PubMed

CITATIONS

229

READS

458

7 authors, including:



[Xiaoyong Deng](#)

Shanghai University

45 PUBLICATIONS 1,776 CITATIONS

[SEE PROFILE](#)



[Yanli Wang](#)

Shanghai University

44 PUBLICATIONS 1,136 CITATIONS

[SEE PROFILE](#)



[Haijiao Zhang](#)

Shanghai University

107 PUBLICATIONS 2,483 CITATIONS

[SEE PROFILE](#)



[Zheng Jiao](#)

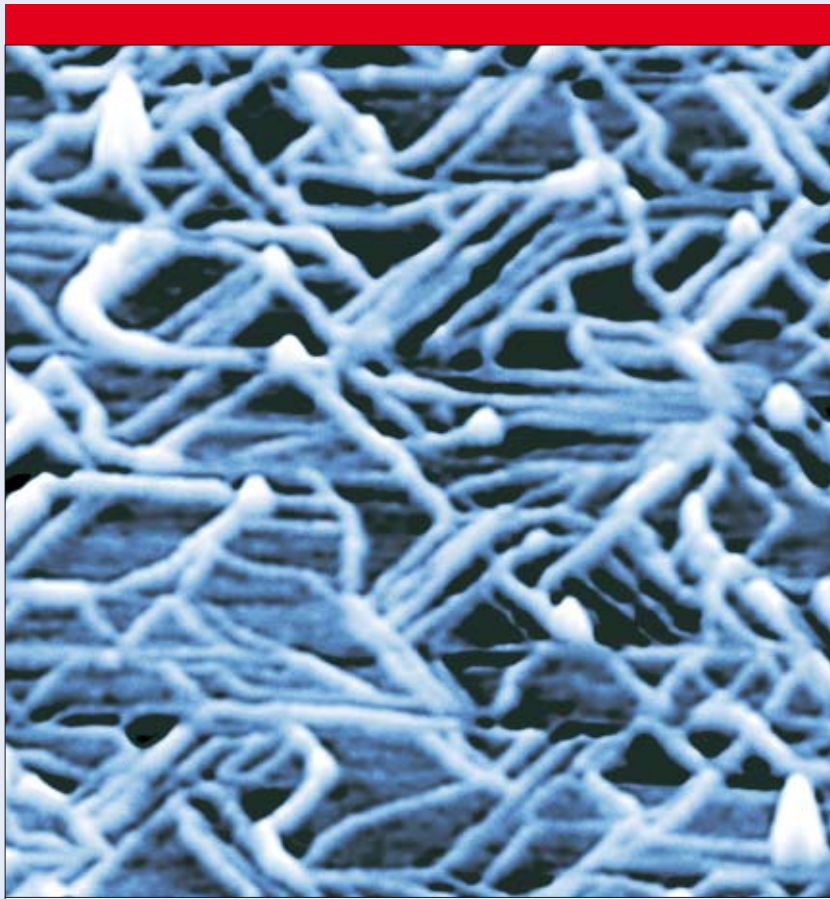
Wuhan University of Science and Technology

155 PUBLICATIONS 3,985 CITATIONS

[SEE PROFILE](#)

NANOTECHNOLOGY

VOLUME 20 NUMBER 10 11 MARCH 2009



www.iop.org/journals/nano

Featured article

Self-assembly of magnetic Ni nanoparticles into
1D arrays with antiferromagnetic order

*V Bliznyuk, S Singamaneni, S Sahoo,
S Polisetty, X He and C Binek*

NANOTECHNOLOGY

Volume 20

Number 11

18 March 2009

PAPERS

Biology and medicine

- 115101 **Nanosized zinc oxide particles induce neural stem cell apoptosis**
Xiaoyong Deng, Qixia Luan, Wenting Chen, Yanli Wang, Minghong Wu, Haijiao Zhang and Zheng Jiao
- 115102 **The interaction of C₆₀ and its derivatives with a lipid bilayer via molecular dynamics simulations**
Robert S G D'Rozario, Chze Ling Wee, E Jayne Wallace and Mark S P Sansom
- 115103 **The influence of surface functionalization on the enhanced internalization of magnetic nanoparticles in cancer cells**
[M] Angeles Villanueva, Magdalena Cañete, Alejandro G Roca, Macarena Calero, Sabino Veintemillas-Verdaguer, Carlos J Serna, Marí a del Puerto Morales and Rodolfo Miranda

Electronics and photonics

- 115201 **Europium doped gallium oxide nanostructures for room temperature luminescent photonic devices**
E Nogales, B Méndez, J Piqueras and J A García

Patterning and nanofabrication

- 115301 **Nanoscale ripples on polymers created by a focused ion beam**
[M] Myoung-Woon Moon, Jun Hyun Han, Ashkan Vaziri, Eun Kyu Her, Kyu Hwan Oh, Kwang-Ryeol Lee and John W Hutchinson
- 115302 **Shrinking solid-state nanopores using electron-beam-induced deposition**
[M] Ronald Kox, Chang Chen, Guido Maes, Liesbet Lagae and Gustaaf Borghs
- 115303 **Large area interference lithography using a table-top extreme ultraviolet laser: a systematic study of the degree of mutual coherence**
P Zuppella, D Luciani, P Tucceri, P De Marco, A Gaudieri, J Kaiser, L Ottaviano, S Santucci and A Reale

Quantum phenomena

- 115401 **A fully coherent electron beam from a noble-metal covered W(111) single-atom emitter**
Che-Cheng Chang, Hong-Shi Kuo, Ing-Shouh Hwang and Tien T Tsong

Sensing and actuating

- 115501 **High sensitivity SnO₂ single-nanorod sensors for the detection of H₂ gas at low temperature**
Hui Huang, Y C Lee, O K Tan, W Zhou, N Peng and Q Zhang
- 115502 **Direct conductance measurements of short single DNA molecules in dry conditions**
Diana Dulić, Sampo Tuukkanen, Chia-Ling Chung, Antoine Isambert, Pascal Lavie and Arianna Filoramo

Materials: synthesis or self-assembly

- 115601 **The surface microstructure controlled growth of organic nanofibres**
Morten Madsen, Jakob Kjelstrup-Hansen and Horst-Günter Rubahn
- 115602 **The effect of GaAs(100) surface preparation on the growth of nanowires**
S C Ghosh, P Kruse and R R LaPierre
- 115603 **Template-free synthesis of BiVO₄ nanostructures: I. Nanotubes with hexagonal cross sections by oriented attachment and their photocatalytic property for water splitting under visible light**
[S] Lu Ren, Lei Jin, Jian-Bo Wang, Fan Yang, Ming-Qiang Qiu and Ying Yu
- 115604 **The photochemical growth of silver nanoparticles on semiconductor surfaces—initial nucleation stage**
S Dunn, S Sharp and S Burgess
- 115605 **The role of surface species in chemical vapor deposited carbon nanotubes**
Andrew C Lysaght and Wilson K S Chiu
- 115606 **Synthesis and room-temperature ferromagnetism of CeO₂ nanocrystals with nonmagnetic Ca²⁺ doping**
Xiaobo Chen, Guangshe Li, Yiguo Su, Xiaoqing Qiu, Liping Li and Zhigang Zou

- 115607 Low-temperature vapour-liquid-solid (VLS) growth of vertically aligned silicon oxide nanowires using concurrent ion bombardment**
Martin Bettge, Scott MacLaren, Steve Burdin, Jian-Guo Wen, Daniel Abraham, Ivan Petrov and Ernie Sammann
- 115608 The preparation of LiCoO₂ nanoplates via a hydrothermal process and the investigation of their electrochemical behavior at high rates**
Xi Qian, Xi Cheng, Zhiyu Wang, Xiaojun Huang, Rui Guo, Dali Mao, Chengkang Chang and Weijie Song
- Materials: properties, characterization or tools**
- 115701 Quantifying the size-dependent effect of the residual surface stress on the resonant frequencies of silicon nanowires if finite deformation kinematics are considered**
Harold S Park
- 115702 Modeling the environmental stability of FeS₂ nanorods, using lessons from biomineralization**
[S] Amanda S Barnard and Salvy P Russo
- 115703 Scanning thermal imaging by near-field fluorescence spectroscopy**
Elika Saïdi, Benjamin Samson, Lionel Aigouy, Sebastian Volz, Peter Löw, Christian Bergaud and Michel Mortier
- 115704 The thermal conductivity and thermal rectification of carbon nanotubes studied using reverse non-equilibrium molecular dynamics simulations**
Mohammad Alaghemandi, Elena Algaer, Michael C Böhm and Florian Müller-Plathe
- 115705 The elastic moduli of oriented tin oxide nanowires**
Sven Barth, Catalin Harnagea, Sanjay Mathur and Federico Rosei
- 115706 The analytical relations between particles and probe trajectories in atomic force microscope nanomanipulation**
A Rao, E Gnecco, D Marchetto, K Mougín, M Schönenberger, S Valeri and E Meyer
- 115707 Phonons in bulk CdSe and CdSe nanowires**
Marcel Mohr and Christian Thomsen
- 115708 Resolving microscopic interfaces in Si_{1-x}Ge_x alloy nanowire devices**
[S] Eun-Kyoung Jeon, Hyunsang Seo, Chi Won Ahn, Hankyu Seong, Heon Jin Choi, Ju-Jin Kim, Ki-jeong Kong, Gyoung-ho Buh, Hyunju Chang and Jeong-O Lee
- 115709 First-principles study of structural and electronic properties of B_xN_yC_z nanocones**
S Azevedo and M Machado



Indicates an article with supplementary data files; see www.iop.org/journals/nano.



Indicates an article with additional multimedia files; see www.iop.org/journals/nano.

Nanosized zinc oxide particles induce neural stem cell apoptosis

Xiaoyong Deng¹, Qixia Luan¹, Wenting Chen², Yanli Wang²,
Minghong Wu^{1,2,3}, Haijiao Zhang¹ and Zheng Jiao¹

¹ Institute of Nanochemistry and Nanobiology, Shanghai University, Shanghai 200444, People's Republic of China

² School of Environmental and Chemical Engineering, Shanghai University, Shanghai 200444, People's Republic of China

E-mail: mhwu@staff.shu.edu.cn

Received 18 September 2008, in final form 8 December 2008

Published 24 February 2009

Online at stacks.iop.org/Nano/20/115101

Abstract

Given the intensive application of nanoscale zinc oxide (ZnO) materials in our life, growing concerns have arisen about its unintentional health and environmental impacts. In this study, the neurotoxicity of different sized ZnO nanoparticles in mouse neural stem cells (NSCs) was investigated. A cell viability assay indicated that ZnO nanoparticles manifested dose-dependent, but no size-dependent toxic effects on NSCs. Apoptotic cells were observed and analyzed by confocal microscopy, transmission electron microscopy examination, and flow cytometry. All the results support the viewpoint that the ZnO nanoparticle toxicity comes from the dissolved Zn²⁺ in the culture medium or inside cells. Our results highlight the need for caution during the use and disposal of ZnO manufactured nanomaterials to prevent the unintended environmental and health impacts.

(Some figures in this article are in colour only in the electronic version)

1. Introduction

Nanotechnology involves the creation and manipulation of materials at the nanoscale level to produce unique products with novel properties. Man-made nanoparticles (NPs) and materials are being rapidly produced in large quantities throughout the world [1]. In the past ten years, many studies have suggested that nanomaterials have different toxicity profiles compared with larger particles because of their small size and high reactivity. As more and more nanomaterials occur in our daily life, there is a serious lack of information concerning the human health and environmental implications of these manufactured nanomaterials [2].

Among many kinds of nanomaterials, ZnO NPs promise to have great benefits for society, and they have been applied in broad fields, including sunscreens, biosensors, food additives, pigments, rubber manufacture, and electronic materials [3]. Furthermore, because of their antibacterial activity, the ZnO NPs have potential applications in prophylactic drugs against bacterially related infections and diseases. Many

published papers have studied the influence of ZnO NPs on microorganisms [4–8]. For example, Adams *et al* [4], Brayner *et al* [5], and Zhang *et al* [6] found that ZnO NPs had significant growth inhibition on *E. coli*; Roselli *et al* showed there were some benefits caused by ZnO in protecting intestinal cells from damage caused by enterotoxigenic *E. coli* [7]; Huang *et al* indicated that ZnO NPs had a good bacteriostasis effect based on *Streptococcus agalactiae* and *Staphylococcus aureus*, which are two etiological agents of several infective diseases in humans [8]. However, only a few studies have investigated the toxicity of ZnO on mammalian cells, and they have resulted in conflicting evidences. Gojova *et al* investigated the cytotoxicity of ZnO NPs with lengths of 100–200 nm and diameters of 20–70 nm, and they showed that about 50% of human aortic endothelial cells died after being incubated with ZnO NPs at a concentration of 50 ppm for 4 h [9]. Similarly, using mouse neuroblastoma cells as the model, Jeng and Swanson found that 50 nm ZnO NPs at a dose of 100 ppm caused 50% of the cells to become dead [10]. Brunner *et al* also found that virtually all mesothelioma MSTO-211H or rodent 3T3 fibroblast cells died after being incubated with 19 nm ZnO NPs at concentrations

³ Author to whom any correspondence should be addressed.

above 15 ppm for 72 h [11]. But Reddy *et al* showed that 13 nm ZnO NPs were only slightly toxic to human T cells at a concentration below 5 mM for 24 h [12].

Recently, there have been an increasing number of reports that NPs can reach the brain and may be associated with neurodegenerative diseases [13, 14]. Oberdörster *et al* indicated that NPs may be taken up directly to the brain from the olfactory epithelium to the olfactory bulb via the olfactory nerves [15]. Previous studies have showed that zinc-containing compounds have neurotoxic effects on the olfactory neuroepithelium; and the dissolved Zn^{2+} from zinc-containing compounds would more easily affect the function of neuro cells, causing neurotoxicity [16, 17]. The neural stem cell (NSC) is a kind of neural precursor cell which possesses the ability of self-renewal and multi-potential differentiation. NSCs exist not only in the developing mammalian nervous system but also in the adult nervous system of all mammalian organisms, including humans. NSCs play an important role in replenishing the lost neurons, and the failure of endogenous NSCs to respond appropriately and the inability of replacing lost neurons might be the cause of neurodegenerative diseases [18]. Herein, we investigate the cytotoxicity of ZnO NPs in mouse NSCs. A CCK-8 assay was used to evaluate the cell viability on treatment with ZnO NPs. Flow cytometry, confocal microscopy, and transmission electron microscope (TEM) analyses were adopted to investigate the cellular morphology and cell apoptosis.

2. Materials and methods

2.1. Characterization of ZnO NPs

Four types of ZnO particles were supplied from commercial companies. ZnO NPs (10 nm) were purchased from Shenzhen Junye Nanomaterials Corp., China; ZnO (30 nm) was purchased from Merk Corp., Germany; ZnO (60 nm) was purchased from Taisheng Corp., China; and ZnO (200 nm) was purchased from Beijing Chemical Reagents Corp., China.

Under dry conditions, the particle crystal structure and specific surface area were analyzed by x-ray diffraction (XRD) and Brunauer–Emmett–Teller (BET) analysis. To prepare an XRD sample, an ethanol suspension containing the metal oxide particles was deposited drop-wise on a single crystal silicon substrate and dried to obtain a thin layer of the particles. The XRD samples were then analyzed in a D/Max-2550 x-ray diffractometer (Rigaku Corp., Tokyo, Japan). The XRD patterns were analyzed using the MDI Jade 6.5 program (Materials Data Inc., California, USA). The BET analysis was conducted on a Gemini 2360 instrument (Micromeritics Instrument Corp., Georgia, USA). The sample was first degassed at 300 °C to reach a pressure $<10 \mu\text{m Hg}$ to remove adsorbed water. The specific surface area of the NP samples was then measured by N_2 adsorption/desorption.

Under aqueous conditions, the particle shape, size, size distribution, and surface charge were studied by TEM (JEM 200CX, JEOL Corp., Tokyo, Japan), dynamic light scattering (DLS, ZetaSizer 3000HSA, Malvern Instruments Ltd., Worcestershire, UK) and electrophoresis. Concentrated

suspensions of ZnO particles (20 ppm) were first prepared with or without 30 min sonication (B5500S-DTH, Branson Ultrasonics Corp., Shanghai, China) in PBS or complete Dulbecco's Modification of Eagle's Medium (DMEM, including 10% fetal bovine serum and 5% horse serum) and stored for 2 h before characterization. All suspensions were vigorously shaken prior to analysis to break up visible clumps and resuspend any sedimentary ZnO particles. The particle shapes and sizes were examined by TEM. Microfilms were prepared by depositing a drop of the respective particle suspension onto a 300-mesh carbon-coated copper specimen grid and drying at room temperature overnight. All sample analyses included at least four different magnifications (10 000, 30 000, 50 000, and 100 000) and at least five fields of view. The particle size distribution and surface zeta-potential were assessed by a ZetaSizer 3000HSA (Malvern Instruments Ltd, Worcestershire, UK). DLS and zeta-potential measurements of ZnO particles were performed in a PBS suspension at pH 7.2 as well as in complete DMEM at pH 7.4.

2.2. ZnO NP suspension preparation and cell culture

ZnO NPs suspension was first acquired by dispersing ZnO NPs in PBS by 30 min sonication at a concentration of 500 ppm. Prior to the next cell experiment, the stock suspension was sonicated again for 15 min and diluted by complete DMEM to the desired concentration.

Mouse NSC line (C17.2) was cultured and maintained in complete DMEM at 37 °C in a cell incubator under a humidified atmosphere with 5% CO_2 . After reaching 85% confluence, cells were transferred to plastic 96-well plates or culture dish.

2.3. Cell viability assay

Cell viability was assessed at 24 h postexposure to ZnO NP suspensions by measuring the conversion of the tetrazolium salt (WST-8) to formazan according to the manufacturer's instructions (CCK-8; Dojindo, Kumamoto, Japan) [19]. Briefly, cells in DMEM were plated onto 96-well plates (about 3000 cells/well). Twelve hours after seeding the cells, each well was treated with a different type of ZnO NP for 24 h, with the final concentration of 0, 3, 6, 12, 18, or 24 ppm. At the end of each time point, 10 μl WST-8 solution was added to each well, and the plates were incubated for an additional 1.5 h at 37 °C. The absorbance of each plate at 450 nm represented a direct correlation with the cell number in this analysis, and was measured by a standard microplate reader (Thermo, Varioskan Flash). Each experiment was done in quadruplicate. The result was expressed with relative cell activity (%) calculated by $[A]_{\text{test}}/[A]_{\text{control}} \times 100$, where $[A]_{\text{test}}$ was the absorbance of the test sample and $[A]_{\text{control}}$ was the absorbance of the control sample without ZnO NPs.

In order to compare the cytotoxicity between the ZnO particles and zinc ions, the viability of NSCs exposed to ZnCl_2 with the concentration of 0.625, 1.25, 2.5, 5, 10, or 24 ppm was also assessed by CCK-8. The IC₅₀ values (i.e., the inhibitory concentration giving a 50% reduction in algal growth rate after 24 h compared to the controls) of ZnO particles and ZnCl_2

Table 1. Hydrodynamic diameter of ZnO NPs (20 ppm) in complete DMEM (pH = 7.4) or PBS (pH = 7.2) determined by dynamic light scattering ($T = 25^\circ\text{C}$).

Dispersant	Treatment	Hydrodynamic diameter ^a (nm) of ZnO NPs			
		10 nm	30 nm	60 nm	200 nm
DMEM	Sonicated	320 ± 191	268 ± 308	221 ± 61	571 ± 220
PBS	Sonicated	582 ± 146	Failed QC ^b	741 ± 257	539 ± 146
	Unsonicated	Failed QC ^b	Failed QC ^b	Failed QC ^b	Failed QC ^b

^a On the basis of the intensity distribution and ten separate measurements per sample.^b QC: instrument-defined quality criteria.

were calculated using a curve fitting method analysis (SPSS Version 13.0, SPSS Inc., Illinois, USA).

2.4. TEM observation

TEM analysis of sample thin sections allows direct visualization of morphological changes. Briefly, after NSCs were grown in culture medium at 37°C for 12 h, ZnO NPs (10 nm) in PBS were added to the well with the final ZnO concentration of 15 ppm and incubated for additional 24 h. Then the cells were fixed in 2.5% glutaraldehyde at 4°C for 2 h, scraped from the flasks and centrifuged at 3000 rpm min^{-1} for 5 min. Next, the sedimentary NSCs were washed with PBS, prefixed with 1% glutaraldehyde at 4°C overnight, and finally postfixed with 1% osmium tetroxide at 4°C for 3 h. After a stepwise dehydration in ethanol, the cells were embedded in epoxy resin for ultrathin sectioning. A slice with about 50 nm thickness was stained with uranyl acetate and lead citrate for subsequent TEM examination.

2.5. DNA fluorescent staining

The fluorescent probe 4,6-diamidino-2-phenylindole (DAPI) is a popular nuclear counterstain for use in multicolor fluorescent techniques. It stains nuclei specifically, with little or no cytoplasm labeling [20]. Cells treated with 15 ppm ZnO NPs (10 nm) for 24 h were collected and sequentially washed by PBS and DAPI working solution. Then, the cells were kept in a $2\text{ }\mu\text{g ml}^{-1}$ DAPI working solution for 15 min in the dark at room temperature. Finally, the cells were washed twice with PBS to remove excess DAPI and examined under a confocal microscope (FV1000, Olympus Corp., Tokyo, Japan) with excitation wavelength of 405 nm. Nuclei are considered to have the normal phenotype when glowing bright and homogeneously. Apoptotic nuclei can be identified by the condensed chromatin gathering at the periphery of the nuclear membrane or a total fragmented morphology of nuclear bodies.

2.6. Annexin V-FITC and PI assay

An Annexin V-FITC and PI assay was employed to detect apoptotic and necrotic cells. Stained cells were analyzed by two-color flow cytometry [21]. The assay procedure is according to the instruction of Annexin V-FITC apoptosis detection kit I (Catalog No. 556547, BD Biosciences, USA). After ZnO treatments, the NSCs were harvested, washed twice with cold PBS (0.15 M, pH 7.2), and resuspended to $1 \times 10^6\text{ cells ml}^{-1}$ in binding buffer. Then, 100 μl of NSCs was transferred to

a 5 ml culture tube and added to by 5 μl of FITC-conjugated Annexin V (Annexin V-FITC) and 5 μl of propidium iodide (PI) at room temperature in the dark. After incubation for 15 min at room temperature in the dark, stained NSCs were diluted by the same binding buffer and directly analyzed by the fluorescence-activated cell sorting method (FACS, FACSCalibur, BD Biosciences, USA). A fluorescence intensity of Annexin V-FITC or PI more than 100 means positive. The positive of Annexin V-FITC indicates the out-releasing of phospholipid phosphatidylserine (PS) which begins in the early stage of apoptosis. The positive of PI indicates the damage of cell membrane, which occurs either in the end stage of apoptosis, in necrosis or in dead cells. In this case, the apoptotic cells were identified as Annexin V-FITC⁺ and PI⁻. The nonviable cells were identified as Annexin V-FITC⁺ and PI⁺ and viable cells were identified as Annexin V-FITC⁻ and PI⁻.

3. Results and discussion

3.1. Characterization of ZnO NPs

Sound research on the toxicity of NPs requires appropriate characterization of the material and basic physicochemical information. The as-prepared ZnO NPs are >99.0% in purity, and with zincite crystal structure. The specific surface area of 10, 30, 60, and 200 nm ZnO NPs is 51.1, 12.9, 8.6, and $4.6\text{ m}^2\text{ g}^{-1}$, respectively.

TEM images of ZnO NPs at concentrations of 20 ppm are shown in figure 1. The figure obviously reveals that ZnO NPs have various shapes, and the width size of a single ZnO NP in each sample is about 10, 30, 60, and 200 nm. However, considerable particle aggregation was observed for each preparation, resulting in the formation of flocs of variable sizes from a few hundred nanometers to several microns in diameter. Compared to the unsonicated samples, there were a number of smaller particles in the sonicated samples. This means that the use of high-power sonication assisted in breaking up the larger ZnO flocs to smaller discrete aggregates, although the primary particles were never isolated under the experimental conditions used.

Using DLS, wide distributions of particle size were observed, all of which were considerably larger than the nominal size of a single ZnO NP (table 1), and in agreement with the TEM measurements. The addition of ZnO NPs to the aqueous medium without sonication resulted in visible flocs in 2 h, and the particle size was so large that they exceeded the instrument-defined quality criteria. By contrast,

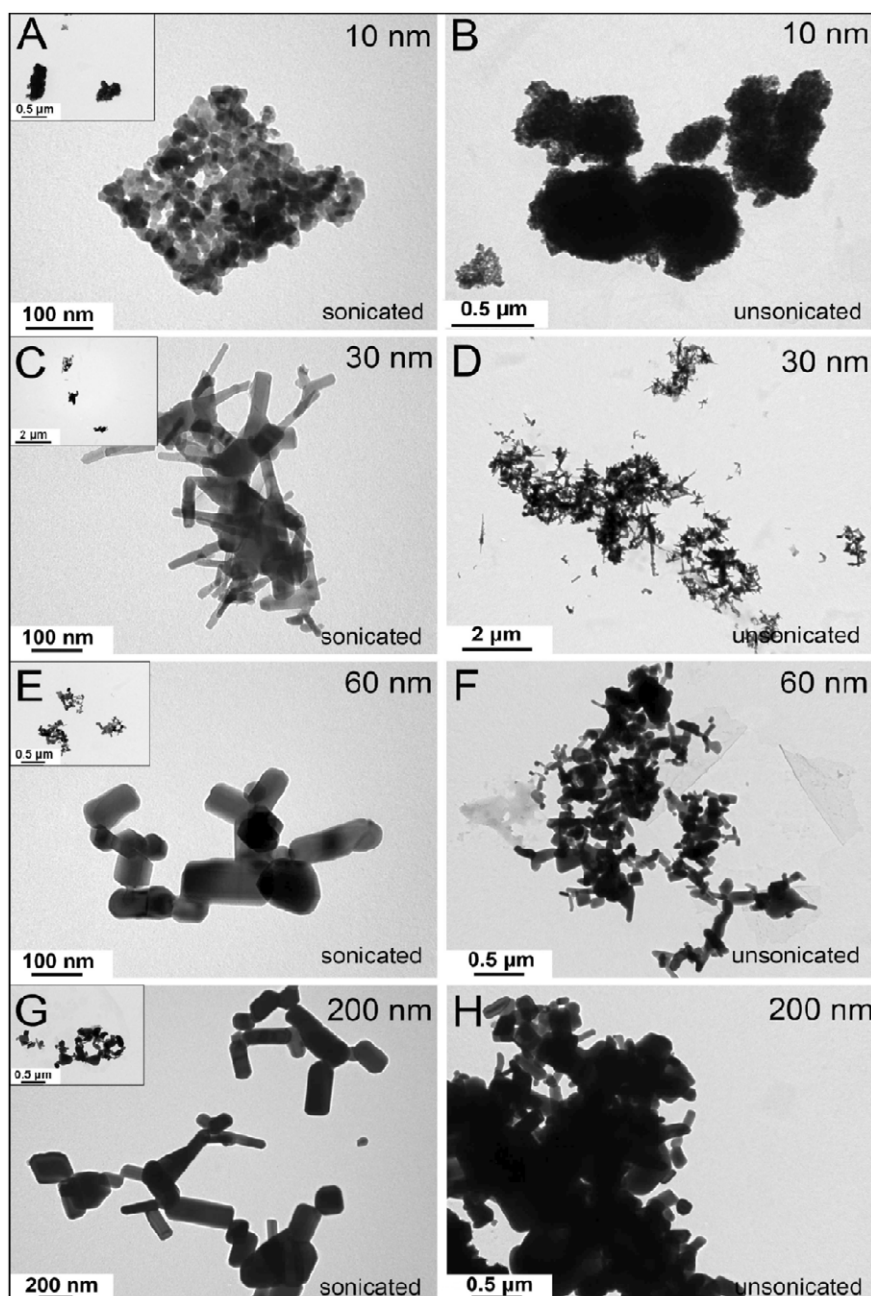


Figure 1. TEM images of ZnO nanoparticles (20 mg l^{-1}) in PBS ($\text{pH} = 7.2$). (A), (C), (E), and (G) in the left column are the sonicated ZnO NPs, and the inset picture illustrates the same sample but at a lower magnification. (B), (D), (F), and (H) in the right column are the unsonicated ZnO NPs.

the sonicated suspension of ZnO NPs did not appear as visible flocs. Interestingly, the particle size in water is larger than that in complete cell culture medium which contains salts, serum proteins, and growth factors that could play a role in particle dispersion and dissolution. The TEM image (figure 2) and particle zeta-potential change (table 2) confirmed that ZnO NPs in complete cell culture medium could absorb some growth factors and proteins.

3.2. Cytotoxicity of ZnO NPs

CCK-8 is widely used to assess cell viability in toxicology tests. Figure 3 shows the cell viability of NSCs incubated with

Table 2. Zeta-potential (mV) of ZnO NPs (20 ppm) dispersed in complete DMEM ($\text{pH} = 7.4$) or PBS ($\text{pH} = 7.2$) by sonication ($T = 25^\circ\text{C}$).

Dispersant	Zeta-potential (mV) of ZnO NPs			
	10 nm	30 nm	60 nm	200 nm
DMEM	-7.0 ± 3.0	-6.8 ± 1.9	-6.0 ± 1.4	-7.0 ± 1.6
PBS	-22.3 ± 1.3	-18.9 ± 1.0	-17.7 ± 1.4	-21.7 ± 1.1

different sizes of ZnO NPs at the concentrations of 3, 6, 12, 18, or 24 ppm for 24 h. No toxic effects were observed for NSCs exposed to below 6 ppm after 24 h. However, a significant

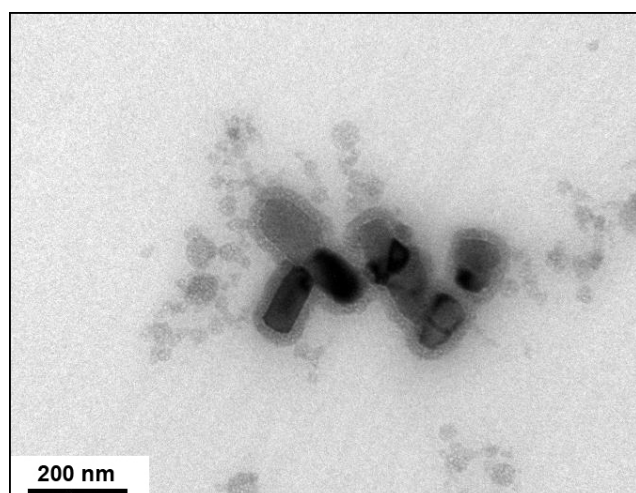


Figure 2. TEM image of ZnO NPs (30 nm, 20 mg l⁻¹) in complete DMEM (pH = 7.4). There are some proteins surrounding the ZnO NPs.

toxic effect was found at the exposed dose above 12 ppm after 24 h. A dose above 24 ppm ZnO NPs causes almost all NSCs to become dead after 24 h co-incubation. The sharp dose-dependent toxicity of ZnO NPs is similar to the result of the work done by Brunner *et al*, who found that the 19 nm ZnO NPs had sharp dose-dependent effects on MSTO or 3T3 cells and that concentrations above 15 ppm would drastically damage all cells post 72 h exposure [11].

The parameter of particle size is usually considered when investigating the toxicity of NPs. Generally, the biological activity of particles increases as the particle size decreases. Smaller particles occupy less volume, resulting in a larger number of particles with a greater surface area per unit mass and increased potential for biological interaction [22]. However, there is no obviously size-dependent toxicity of ZnO NPs observed in this work. There are two reasons that could result in this phenomenon. First, ZnO NPs with different size dispersed in complete DMEM easily aggregate to form large particles with similar size (table 1). The other reason is that the toxicity of ZnO NPs may ascribe mainly to the dissolved zinc ions in the medium. In order to prove this mechanism, we studied the NSC toxicity of ZnCl₂ and determined whether the ZnO NP toxicity differed from that of ionized Zn²⁺. Table 3 is the 24 h IC₅₀ values of ZnO NPs and ZnCl₂; these comparable values show that ZnO NPs and ZnCl₂ have similar toxic effects on NSCs. In fact, some previous studies have revealed a similar result [11, 23, 24]. Brunner *et al* first inferred that the sharp dose-dependent toxic effects of ZnO NPs on MSTO or 3T3 cells may be attributed to the release of Zn²⁺ ions before or after uptake into the cells [11]. Then Franklin *et al* found a comparable toxicity of nanoparticulate ZnO, bulk ZnO, and ZnCl₂ to the freshwater alga *Pseudokirchneriella subcapitata* and attributed the ZnO NP toxicity solely to dissolved zinc [23]. Very recently, Xia *et al* thoroughly investigated the mechanism of *in vitro* toxicity of ZnO, TiO₂, and CeO₂ NPs [24]. They showed that ZnO dissolution could happen in culture medium and reach >80%

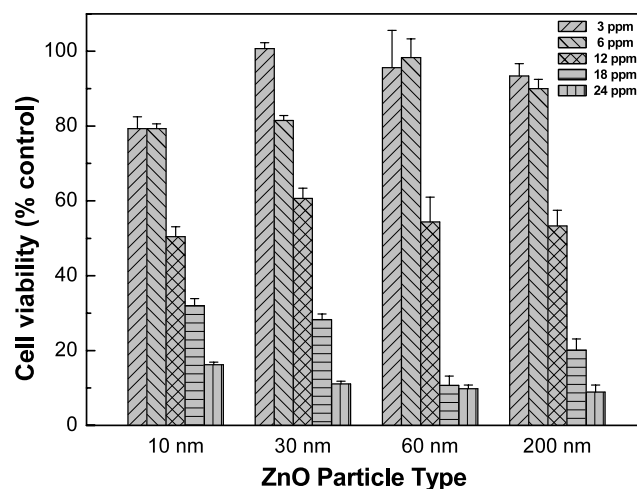


Figure 3. Cell viability of NSCs co-incubated with different sized ZnO NPs for 24 h via CCK-8 assay. Control cells treated without ZnO NPs are considered to have 100% activity. Results are expressed as a percentage of control and mean \pm SEM (standard error of the mean) of four culture dishes.

Table 3. The 24 h IC₅₀ (95% confidence limits) values for neural stem cells exposed to different sized ZnO or ZnCl₂. Data are calibrated to Zn concentrations.

	ZnO				ZnCl ₂
	10 nm	30 nm	60 nm	200 nm	
Zn concentration (ppm)	9.3–11.3	9.4–10.8	10.8–13.2	10.2–13.5	6.7–8.3

of the maximum total concentration of dissolved Zn²⁺ ions within 3 h, and thus expected that the cell cultures were mainly exposed to aqueous Zn ions when less than maximum concentration of ZnO NPs was used. They estimated that the maximum total dissolved zinc concentrations could be 225 μ M in complete DMEM (corresponding to 18.2 ppm ZnO dissolved). Therefore, when less than the maximum concentration of ZnO NPs (about 18 ppm) is used, we expect that the cells are mainly exposed to aqueous Zn ions, but when particle concentrations are used that exceed the ZnO solubility, the cells will be exposed to non-dissolved NPs.

3.3. TEM observation

In order to further investigate the damage and fate of NSCs treated by ZnO NPs, TEM examination of sample thin sections was used to directly view the ultramorphological changes of NSCs. Figure 4 is a representative TEM image of NSCs treated with or without 10 nm ZnO NPs. Control NSCs present normal structure and no damages are observed (figure 4(A)). However, most NSCs treated by ZnO NPs are apoptotic, with changed morphology, condensed chromatin, blebbing, and damaged or disappeared organelles (figures 4(B) and (C)). An early apoptosis cell is shown in figure 4(B), which indicates that the apoptotic process starts with the condensation of chromatin at the nuclear periphery, formation of many blebs, and emerged swollen or hollow mitochondria. An advanced apoptosis cell is

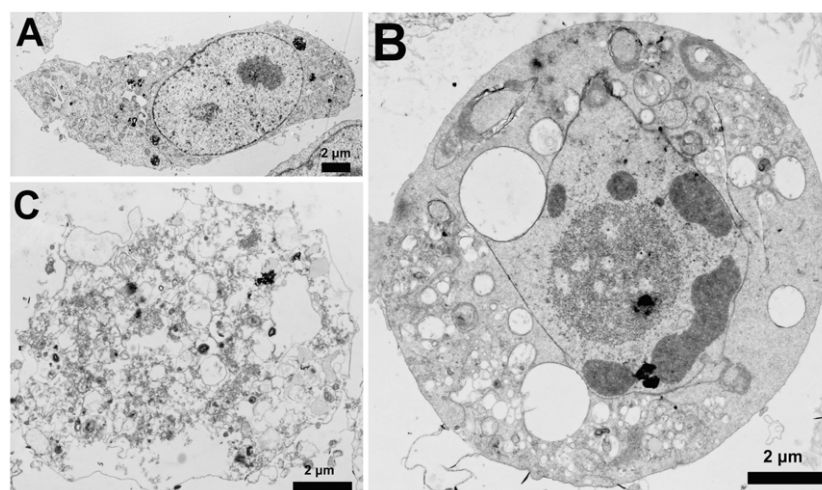


Figure 4. TEM images of control NSCs (A) and early (B) or advanced (C) apoptotic NSCs treated with 15 ppm ZnO NPs (10 nm) for 24 h.

shown in figure 4(C), which indicates that the NSC nucleolus and organelles are totally damaged and cracked, but the plasma keeps intact. Here, we note that the engulfed ZnO NPs are very hard to be visualized in the damaged NSCs and this probably comes from the ZnO NPs dissolved in DMEM or cell lysosomes. This result confirms again that the toxicity of ZnO NPs is mainly from the dissolved zinc ions.

3.4. DNA fluorescent staining

In general, the mechanism of neurotoxicity by zinc involves necrosis or apoptosis. Therefore, apoptosis could be one fate of NSCs treated by ZnO NPs. Figure 5 shows representative morphology and DAPI-fluorescence photographs of control NSCs and treated NSCs after 24 h exposure to 15 ppm ZnO NPs (10 nm). In the control group (figures 5(A) and (B)), NSCs grow exuberantly, with integrated nucleus structure, nucleolus, and clearly distinguished karyothecas, and the contents in the nucleus are homogeneous. But in the ZnO group, all cells have undergone morphological changes to nearly spherical shape, have gained in volume, and have lost adhesion to the cell culture dish (figure 5(C)). Figure 5(D) shows hypercondensed chromatin at the nuclear periphery in most NSCs, and this means that these NSCs are under an apoptotic process. Again, there are no ZnO NPs observed under the microscope, and this also confirms that most of ZnO NPs are dissolved in the culture medium.

3.5. Apoptosis and necrosis of NSCs

In order to quantitatively analyze apoptotic and necrosis NSCs under ZnO treatment, Annexin V-FITC and PI assay plus FACS technology were employed. In the control group, no apoptosis happened after 24 h cultivation (figure 6(A)). However, when the cells were treated with ZnO NPs, the numbers of apoptotic and necrosis cells increased markedly (figures 6(A) and (B)). Furthermore, as the exposure time was prolonged from 3 to 24 h, the total number of apoptotic cells increased from 18.2% to 55.6% (figures 6(B) and (C)). The

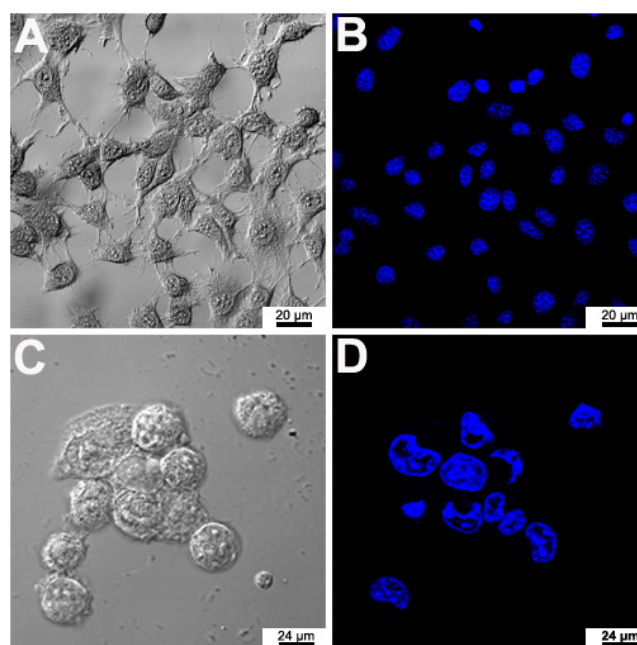


Figure 5. Differential interference contrast images ((A) and (C)) and fluorescent images ((B) and (D)) of NSCs examined under a laser scanning confocal microscope. (A) and (B) are control cells, while (C) and (D) are NSCs after 24 h exposure to 10 nm ZnO NPs at the concentration of 12 ppm. The hypercondensed chromatin at the nuclear periphery in ZnO-treated cells means that ZnO NPs can induce NSCs to become apoptotic.

apoptosis or necrosis pathway of NSCs caused by ZnO NPs is not yet clear. However, it should be noted that mitochondria are the primary target in Zn^{2+} neurotoxicity and Zn^{2+} can inhibit mitochondrial respiration at different points [25]. Marin *et al* showed that a number of the enzymes required for mitochondrial respiration are inhibited, and that brief exposure to $100 \mu\text{M}$ Zn^{2+} caused a 50% loss of intracellular ATP [26]. In addition, Xia *et al* also revealed that ZnO dissolution could happen in cell endosomes and induced cell toxicity by leading to the generation of reactive oxygen species (ROS), oxidant injury, excitation of inflammation, and cell death [24].

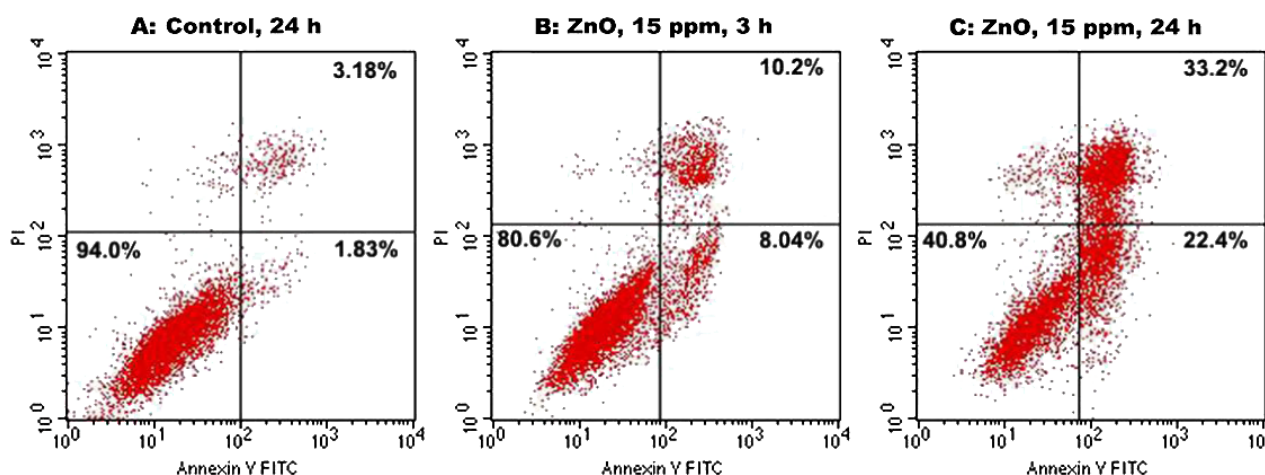


Figure 6. FACS results of the Annexin V-FITC and PI assay. A cell that stains Annexin V-FITC⁺ and PI⁺ is in the upper-right quadrant, one that stains Annexin V-FITC⁺ and PI⁻ is in the lower-right quadrant, and one that stains Annexin V-FITC⁻ and PI⁻ is in the lower-left quadrant. (A) control group with no ZnO treatment; (B) NSCs co-cultured with 10 nm ZnO NPs at the concentration of 15 ppm for 3 h; (C) NSCs co-cultured with 10 nm ZnO NPs at the concentration of 15 ppm for 24 h.

4. Conclusion

In summary, we have presented a preliminary study of the toxicological impact of ZnO NPs on NSCs. The results show that ZnO NPs do not cause any cell damage at lower concentration, but dramatically damage NSCs at a concentration higher than 12 ppm after 24 h exposure. Apoptotic cells were observed and quantitatively analyzed by confocal, TEM, and FACS examinations. The mechanism of NSC toxicity of ZnO NPs was discussed and we concluded that the ZnO NP toxicity mainly comes from the dissolved Zn²⁺ in the culture medium or inside cells. Further studies are needed to develop the necessary safety precautions and exposure limits for people working with these materials and those who might be exposed to these materials when they are implemented in commercial, industrial, and medical applications.

Acknowledgments

The authors are grateful to Professor Yuanfang Liu and Dr Jing Wang from Peking University for kind help. We acknowledge Professor Haifang Wang and Mr Shengtao Yang from Peking University for providing ZnO NPs, the XRD and BET data. We thank Professor Tieqiao Wen from Shanghai University for the gift of neural stem cells. This work was supported by the China 973 project (2006CB705604), China Natural Science Foundation (20871081), the 'Dawn' Program of Shanghai Education Commission (07SG46), Shanghai Natural Science Foundation (08ZR1407800), and Shanghai Leading Academic Disciplines (S30109).

References

- [1] Gerber C and Lang H P 2006 *Nat. Nanotechnol.* **1** 3
- [2] Guzman K A D, Taylor M R and Banfield J F 2006 *Environ. Sci. Technol.* **40** 1401
- [3] Ji S L and Ye C H 2008 *J. Mater. Sci. Technol.* **24** 457
- [4] Adams L K, Lyon D Y and Alvarez P J 2006 *Water Res.* **40** 3527
- [5] Brayner R, Ferrari-Iliou R, Brivois N, Djediat S, Benedetti M F and Fievet F 2006 *Nano Lett.* **6** 866
- [6] Zhang L, Jiang Y, Ding Y, Povey M and York D 2007 *J. Nanopart. Res.* **9** 479
- [7] Roselli M, Finamore A, Garaguso I, Britti M S and Mengheri E 2003 *J. Nutr.* **133** 4077
- [8] Huang Z, Zheng X, Yan D, Yin G, Liao X, Kang Y, Yao Y, Huang D and Hao B 2008 *Langmuir* **24** 4140
- [9] Gojova A, Guo B, Kota R S, Rutledge J C, Kennedy I M and Barakat A I 2007 *Environ. Health Perspect.* **115** 403
- [10] Jeng H A and Swanson J 2006 *J. Environ. Sci. Health A* **41** 2699
- [11] Brunner T J, Wick P, Manser P, Spohn P, Grass P N, Limbach L, Bruinink A and Stark W J 2006 *Environ. Sci. Technol.* **40** 4374
- [12] Reddy K M, Feris K, Bell J, Wingett D G, Hanley C and Punnoose A 2007 *Appl. Phys. Lett.* **90** 213902
- [13] Block M L, Wu X, Pei Z, Li G, Wang T, Qin L, Wilson B, Yang J, Hong J S and Veronesi B 2004 *FASEB J.* **18** 1618
- [14] Peters A, Veronesi B, Calderon-Garciduenas L, Gehr P, Chen L C, Geiser M, Reed W, Rothen-Rutishauser B, Schurch S and Schulz H 2006 *Part. Fibre Toxicol.* **3** 13
- [15] Oberdörster G, Sharp Z, Atudorei V, Elder A, Gelein R, Kreyling W and Cox C 2004 *Inhal. Toxicol.* **16** 437
- [16] Persson E, Henriksson J, Tallkvist J, Rouleau C and Tjalve H 2003 *Toxicology* **191** 97
- [17] Takeda A, Ohnuma M, Sawashita J and Okada S 1997 *Neurosci. Lett.* **225** 69
- [18] Gage F H 2000 *Science* **287** 1433
- [19] Tominaga H, Ishiyama M, Ohseto F, Sasamoto K, Hanamoto T, Suzuki K and Watanabe M 1999 *Anal. Commun.* **36** 47
- [20] Siegel T N, Hekstra D R and Cross G S M 2008 *Mol. Biochem. Parasitol.* **160** 171
- [21] Yang L, Zhou X, Yang J, Yin X, Han L and Zhao D 2008 *J. Neuroimmunol.* **199** 10
- [22] Oberdörster G, Stone V and Donaldson K 2007 *Nanotoxicology* **1** 2
- [23] Franklin N M, Rogers N J, Apte S C, Batley G E, Gadd G E and Casey A S 2007 *Environ. Sci. Technol.* **41** 8484
- [24] Xia T, Kovochich M, Liong M, Madler L, Gilbert B, Shi H, Yeh J I, Zink J I and Nel A E 2008 *ACS Nano* **2** 2121
- [25] Daniels W M U, Hendricks J, Salie R and van Rensburg S J 2004 *Metab. Brain Dis.* **19** 79
- [26] Marin P, Israel M, Glowinski J and Premont J 2000 *Eur. J. Neurosci.* **12** 8